Phase coexistence, magnetic inhomogeneity, and disorder in the charge-ordered state of $Pr_{2/3}Ca_{1/3}MnO_3$

C. Frontera and J. L. García-Muñoz*
Institut de Ciència de Materials de Barcelona, CSIC, Campus de la UAB, E-08193 Bellaterra, Catalonia, Spain

A. Llobet
Laboratoire Louis Néel, CNRS, 38042-BP 166, Grenoble Cedex 9, France

M. Respaud and J. M. Broto
SNCMP and LPMC, INSA, Complexe Scientifique de Rangueil, F-31077 Toulouse, France

J. S. Lord
Isis Facility, RAL Chilton, Didcot, Oxon OX11 0QX, United Kingdom

A. Planes
Departament d'Estructura i Constituents de la Matèria, Facultat de Física, Universitat de Barcelona, Catalonia, Spain
(Received 28 December 1999)

The coexistence of ferromagnetic metallic and antiferromagnetic charge-ordered (CO) states in $Pr_{2/3}Ca_{1/3}MnO_3$ has been investigated using zero-field muon spin relaxation, neutron diffraction, calorimetric, and magnetic measurements. Calorimetric data evidence a high degree of disorder below the CO transition. The data are consistent with large antiferromagnetic (AFM) CO regions containing structural and magnetic inhomogeneities densely scattered. Below the charge order temperature ($T_{CO} \approx 220$ K) the dominant relaxation mechanism of the muon polarization is based on ferromagnetic Mn-Mn correlations and the spin-lattice relaxation rate is peaked at T_C instead of T_N. The results agree with a spatial distribution of ferromagnetic and AFM regions strongly interpenetrated. The presence of local magnetic order in the whole sample is only achieved just below $T_C \approx 120$ K.

I. INTRODUCTION

The very rich phenomena accompanying the structural, magnetic, and transport properties of manganese oxides with perovskite-type structure ($Ln_{1-x}A_xMnO_3$ with Ln≡lanthanide and A≡alkaline earth) have been the subject of a large research effort during the last years. As a direct consequence of the twofold degeneracy of the e_g electrons and the remarkable competition among the relevant interactions, a large variety of ground states are being found in this family of compounds. In addition to the ferromagnetic double exchange interactions, favoring a ferromagnetic ground state, Coulomb repulsion, and Jahn-Teller distortion favor the localization of the charges and the antiferromagnetic coupling of the moments. The tilt of the MnO_6 octahedra when the mean size (R_A) of the cations at the lanthanide site is reduced favors the localization and ordering of the charges. With this, at low temperatures, $La_{0.7}Ca_{0.3}MnO_3$ ($R_A = 1.15$ Å) is ferromagnetic and metallic, while $La_{0.35}Y_{0.35}Ca_{0.3}MnO_3$ ($R_A = 1.10$ Å) presents no net magnetization. In the middle $Pr_{0.7}Ca_{0.3}MnO_3$ ($R_A = 1.12$ Å) presents a charge order transition at 200 K, accompanied by antiferromagnetic order below 150 K and the appearance of a net ferromagnetic moment below 100 K. This last transition was attributed to a canting of the collinear-CE-type magnetic structure below 100 K.[1] In the line of some other evidences for phase separation phenomena between two characteristic states with well defined energy minima, Kiryukhin *et al.*[2] and Cox *et al.*[3] have reported the induction of phase segregation in $Pr_{0.7}Ca_{0.3}MnO_3$ when exposing it to x-ray radiation at low temperatures. The ferromagnetic phase created persists when the exposure disappears and is only removed when the system is annealed above 40 K. This photoinduced phase separation leads to a persistent photoconductivity.[4] Tomioka *et al.* reported[5] that, for a single crystal at low temperature, a fully ferromagnetic metallic state is achieved (first order transition) with the application of a magnetic field of about 4 T. Moreover, the charge order state is not recovered when the field is switched off. Slow thermal relaxation effects from the metastable metallic phase to the insulating CO phase were reported by Anane *et al.* below 50 K.[6] The ferromagnetic metallic state can also be achieved by the application of an electric field,[7] high pressure,[8] irradiation with a laser pulse[9] with visible light,[10] or electrons.[11] In contrast with the final state of $Pr_{0.7}Ca_{0.3}MnO_3$ after x-ray irradiation, the existence of two segregated types of cells of different characteristic volume has not been observed by synchrotron x-ray powder diffraction. Instead the presence of lattice strain was associated with trapped ferromagnetic clusters. In addition, the high level of noise measured recently in the sample $Pr_{2/3}Ca_{1/3}MnO_3$ has been attributed to phase separation.[12]

In the present work we have investigated the nonhomogeneous nature of the charge ordered manganite $Pr_{2/3}Ca_{1/3}MnO_3$. Using neutron diffraction, muon spin relaxation, magnetic, and calorimetric measurements, we present

results that, in particular, contribute to a more precise description and understanding of the spatial distribution of coexisting FM and CO phases in this system with unusual properties.

II. EXPERIMENTAL

Polycrystalline $Pr_{2/3}Ca_{1/3}MnO_3$ ceramics were prepared by conventional solid-state reaction. A mixture of $CaCO_3$, Mn_2O_3, and Pr_6O_{11} at the desired ratio was prefired at 750 °C in air. After some intermediate treatments, the powder was pressed into pellets, fired at 1400 °C for 15 h, cooled to room temperature and ground again for several times. With the purpose of comparing the macroscopic and microscopic or local information we have combined the following types of measurements. Neutron diffraction (ND) measurements were performed at the Lab. Leon Brillouin (Paris) and the Institut Laue-Langevin (Grenoble) using G4.1($\lambda = 2.426$ Å) and D1B($\lambda = 2.52$ Å) diffractometers at different selected temperatures. ND data were analyzed using the program FULLPROF.[13] Differential scanning calorimetric (DSC) measurements have been done using a noncommercial calorimeter.[14] DSC data were taken warming the sample, in the temperature interval $90\,\mathrm{K} \leqslant T \leqslant 340\,\mathrm{K}$. $La_{2/3}Ca_{1/3}MnO_3$ was used as reference sample because it does not present phase transitions below its ferromagnetic critical temperature $T_C = 274$ K. In order to determine the error bars we have also used Pb as a reference sample. A self-consistent method has been used for the determination of the baseline. This method takes into account that the ratio between the thermal power (dQ/dt) and the heating rate (dT/dt) is given by $(dQ/dt)/(dT/dt) = dQ/dT = \Delta C$, where ΔC is the difference between the heat capacities of the sample and the reference. Macroscopic magnetic measurements were performed using a SQUID magnetometer. Muon spin relaxation (μ^+SR) measurements were conducted at the ISIS pulsed muon facility (Rutherford Appleton Laboratory, Chilton, UK) using the MUSR instrument. A 10 g powder sample was mounted on an Al plate with a silver mask in a closed cycle refrigerator, and the measurements made over the temperature range 15–350 K. In these measurements fully polarized positive muons are implanted in the sample. The subsequent evolution of muon polarization occurs in response to the coupling between the muon spin and the internal magnetic fields. The decay of the muon ($\tau_\mu = 2.2\ \mu$s) is accompanied by positron emission preferentially along the muon spin direction. Two rings of positron detectors, with their axis coinciding with the direction of the initial polarization of the muons, are placed at either side of the sample. The resulting positron count rate, collected in time histograms in forward (F) and backward (B) detectors, is used to monitor the evolution of the implanted muon polarization via the relaxation function $G_z(t) = a_0 P(t) = [I_F(t) - \alpha I_B(t)]/[I_F(t) + \alpha I_B(t)]$, where I_F and I_B are the time differential positron counts in the F and B detectors, respectively. α is a calibration factor and a_0 the initial asymmetry.

III. RESULTS

Figure 1 shows the temperature dependence of the integrated ND intensities of some peaks, which have been indexed referred to the *Pbnm* setting. Fig. 1(a) shows the intensity of the superlattice reflection (2 $\frac{3}{2}$ 0), which gives definitive evidence of the development of charge ordered (CO) regions in the sample below ~220 K. As expected the charge order superlattice reflections can be indexed on the basis of a double orthorhombic $ax2bxc$ cell (*Pbnm* setting).[15] The perfect form of this charge order can only be achieved when the fractions of Mn^{3+} and Mn^{4+} ions are equal. The magnetic reflections at positions ($\frac{1}{2}$ 0 0) and ($\frac{1}{2}\frac{1}{2}$ 0) [Fig. 1(b)] appear at $T_N \approx 155$ K and are consistent with the development of a collinear CE-type antiferromagnetic (AFM) structure.[15] This magnetic structure is characterized by two distinguishable manganese positions: Mn(I) with propagation vector ($\frac{1}{2}$, 0, 0) (mainly occupied by Mn^{3+} ions), and Mn(II) with propagation vector ($\frac{1}{2}$, $\frac{1}{2}$, 0) (mainly occupied by Mn^{4+} ions). The integrated intensity of some nuclear reflections [for instance, (0 2 0) and (0 0 2)] [Figs. 1(c), 1(d)] are suddenly enlarged indicating the appearance of some ferromagnetic (FM) order below $T_C \approx 120$ K. Partial FM order of the Pr ions ($\mu_{Pr} = 0.4\mu_B$) has been described below 30 K.[3] Notice that, in Fig. 1(a), the intensity of the superlattice reflection (2 $\frac{3}{2}$ 0) systematically increases when decreasing temperature through the Curie point. According to the calculations, this peak is purely structural in origin with no contribution from AFM order. Figure 1(a) gives evidence that there are no changes in the evolution of this intensity across T_C. Therefore, the crystallization process of CO regions is apparently unaffected by the appearance of static ferromagnetic moments in the sample. A similar conclusion can be drawn from the temperature evolution of ferromagnetic and antiferromagnetic sublattices. Namely, the growth rate of superlattice AFM peaks ($\frac{1}{2}$ 0 0) or ($\frac{1}{2}$ $\frac{1}{2}$ 0) [purely AFM, Fig. 1(b)] is not altered by the freezing of the ferromagnetic component. Figures 1(c) and 1(d) show the development of two

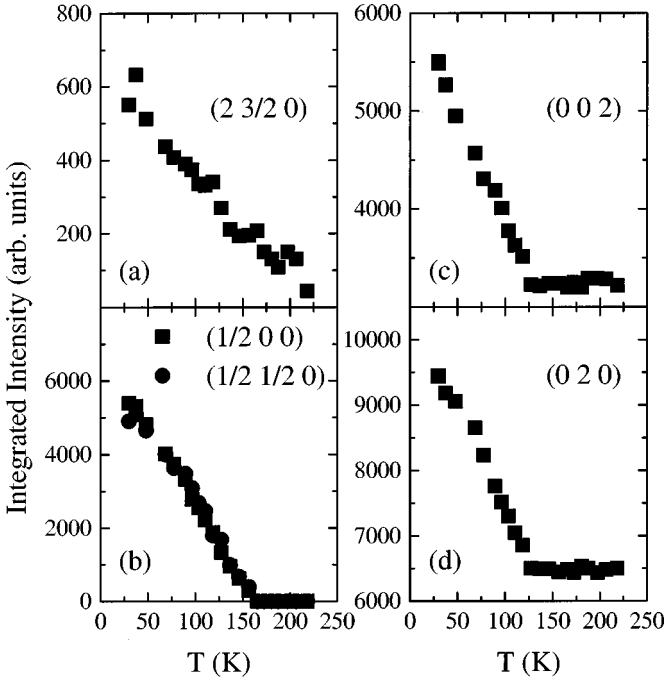

FIG. 1. Thermal evolution of the integrated neutron diffraction intensities for (a) (2 $\frac{3}{2}$ 0) [CO superlattice], (b) ($\frac{1}{2}$ 0 0) and ($\frac{1}{2}$ $\frac{1}{2}$ 0) [AFM CE], (c) (0 0 2), and (d) (0 2 0). (c) and (d) have a contribution from FM ordering and are used to monitor the structural and magnetic transitions.

peaks with a magnetic contribution due to FM freezing. It is clear from these observations that a thermally driven spin reorientation (from a pure collinear CE AFM structure to a canted magnetic ordering) should be completely ruled out in this system.

The picture of two separated magnetic regions is consistent with the observation of large ferromagnetic droplets in $Pr_{0.7}Ca_{0.3}MnO_3$ after exposure to x-ray beam,[2,3] where the ferromagnetic phase has a smaller volume than that of the CO phase.[3] In an attempt of clarifying whether it is or not possible to distinguish different lattices (as would happen in the case of phase separation) to, respectively, FM and AFM ordered regions in $Pr_{2/3}Ca_{1/3}MnO_3$, we performed different sets of Rietveld refinements of the low temperature ND data. Allowing for two differentiated cells, the reliability factors ($R_{wp}=8.4$) did not improve significantly and a clear convergence to two well-defined sets of lattice parameters was not obtained. The ordered magnetic moments obtained from the refinements were $m_{\mathrm{AFM}}(\mathrm{I})=1.9(2)\mu_B$, $m_{\mathrm{AFM}}(\mathrm{II})=1.8(2)\mu_B$, and $m_{\mathrm{FM}}=1.5(3)\mu_B$. Therefore the total ordered moments, $m(\mathrm{I})=2.5$ and $m(\mathrm{II})=2.3\mu_B/\mathrm{ion}$, are clearly below the expected saturation values ($4\mu_B[\mathrm{Mn(I)}]$ and $3.33\mu_B[\mathrm{Mn(II)}]$). Their thermal evolution has been depicted in Fig. 7(a). On the other hand, as expected, the $m_{\mathrm{AFM}}/m_{\mathrm{FM}}$ ratio in our sample with $x=\frac{1}{3}$ is larger than in the samples with lower hole concentration previously reported.[1,3]

One of the purposes of the present work has been to use a local magnetic probe to give insight into the real spatial distribution of the FM ordered regions with respect to the AFM coupled charge-ordered zones. With this objective in mind, μSR spectra were collected in zero external field (ZF) over the temperature range 15–350 K. Longitudinal fields up to 2 kOe were also applied at selected temperatures without appreciable changes in the relaxation. In Fig. 2, we show the evolution of the μSR asymmetry $G_z(t)$ at various temperatures. Single exponential decay [$G_z(t)=a_0\exp(-\lambda t)$] characterizes the depolarization above $T_N\approx 155$ K. λ is the dynamic spin-lattice relaxation rate, proportional to the amplitude of the local field (H_l) fluctuations at the muon site [$\lambda=(\gamma_\mu H_l)^2\tau$; τ being the primary correlation time between fluctuations and γ_μ the gyromagnetic ratio of μ^+]. Below 155 K, a stretched exponential (SE), [$G_z(t)\sim\exp\{-(\lambda_s t)^\beta\}$] function is required to describe the muon decay (solid lines in Fig. 2). The variation with temperature of the SE relaxation rate λ_s and the initial asymmetry (a_0) are shown in Fig. 3. The solid line reproducing $\lambda_s(T)$ above the ferromagnetic transition in this figure is a fit by the function $\lambda_s(T)=\lambda_0(T/T_c-1)^{-\gamma}$ which gives $T_c=120(3)$ K, $\gamma=0.51(1)$, and $\lambda_0=0.066(1)\ \mu\mathrm{s}^{-1}$. This transition temperature agrees very well with that determined from magnetization and neutron measurements. Though this power-law dependence is expected only very close to the Curie transition temperature, it represents a phenomenological description of the relaxation rate above T_c. Moreover, the asymmetry loss below T_N is shown in Fig. 3. The appearance of a spontaneous nonzero static field causes a precession of the muon spin. Because of the pulsed structure of the ISIS beam, the subsequent muon spin rotation falls beyond the accessible frequency window at ISIS (high frequency cutoff). As a result, below the magnetic transition the initial asymmetry a_0 reduces to $\frac{1}{3}$ of its value at higher temperature. Only the component of muon polarization parallel to the local magnetization is preserved. Integrating over all directions in a multidomain or powder sample gives the factor $\frac{1}{3}$.

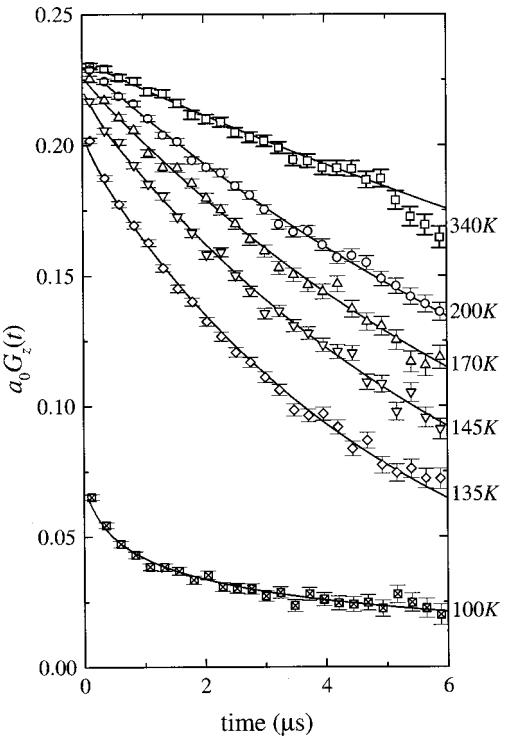

FIG. 2. Time dependence of the ZF muon relaxation spectra at some selected temperatures. Solid lines are fits as explained in the text.

Figure 4(a) shows the DSC thermogram obtained when $La_{2/3}Ca_{1/3}MnO_3$ is used as a reference sample. The area be-

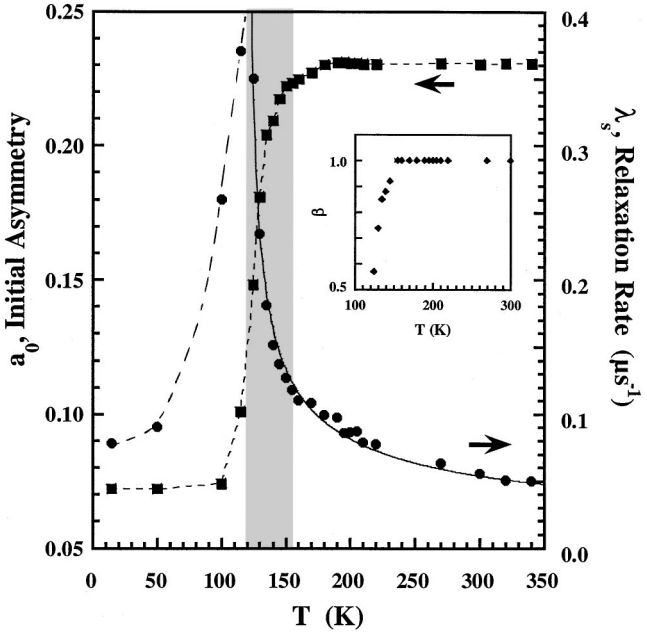

FIG. 3. Temperature dependence (warming) of the fitted relaxation rate λ_S and the initial asymmetry for $Pr_{2/3}Ca_{1/3}MnO_3$. The solid line is a fit to the power-law dependence $\lambda_S(T)=\lambda_0(T/T_c-1)^{-\gamma}$ (see text). The SE exponent β is shown in the inset.

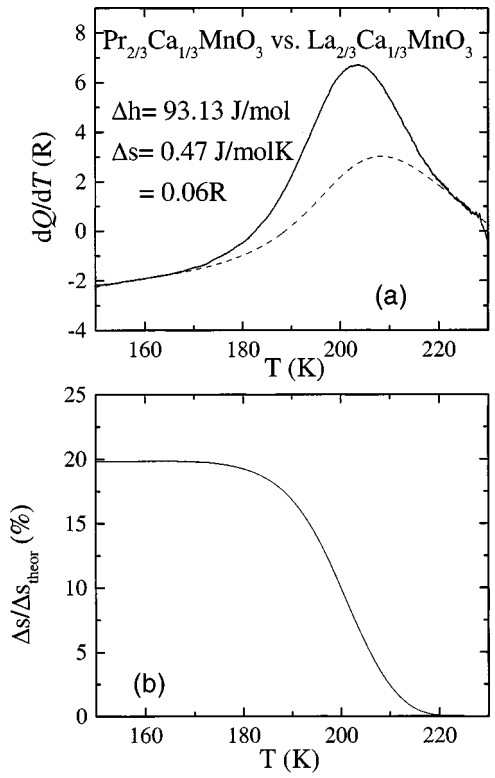

FIG. 4. (a) Heat flow (warming) obtained by DSC using $La_{2/3}Ca_{1/3}MnO_3$ as reference sample and calculated baseline (dashed). (b) Relative (%) entropy change due to the CO transition for $Pr_{2/3}Ca_{1/3}MnO_3$ (referred to the theoretical expected value).

low the peak is $\Delta h \approx 93.1$ J/mole. The measured change in entropy across the transition is $\Delta s \approx 0.06R$. This result was confirmed using Pb as reference sample in additional DSC measurements.

Finally, the effects of the CO and magnetic transitions on the susceptibility (χ) are shown in detail in the Fig. 5. In commensurate $Ln_{1/2}Ca_{1/2}MnO_3$ compounds with separated

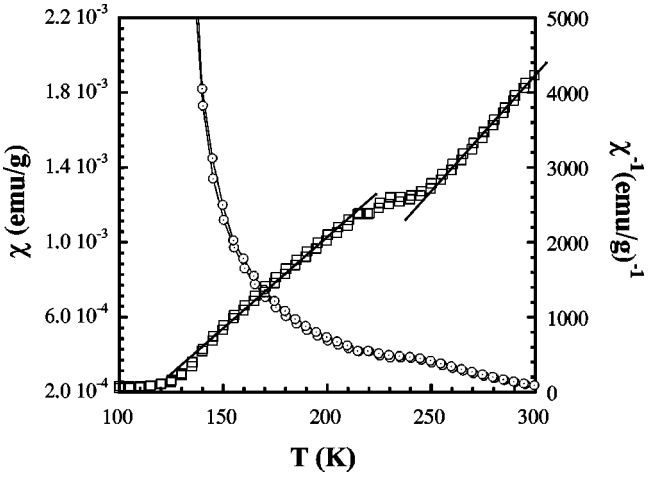

FIG. 5. Detail of the dc susceptibility (open circles) and its inverse (squares) of $Pr_{2/3}Ca_{1/3}MnO_3$ (20 Oe) around the CO transition.

T_N and T_{CO}, the susceptibility decreases when the sample is cooled down through the CO transition. The reason is the switch from FM to AFM correlations that accompanies the electronic reorganization,[16] and the Curie temperature changes its sign from positive to negative. The CO anomaly with $x=\frac{1}{3}$ can be seen in Fig. 5. Although θ_c has decreased below T_{CO}, at variance with the commensurate case, the Curie temperatures estimated at both sides of the transition are both positive: $\theta_C = 170$ K ($T > T_{CO}$) and $\theta_c = 110$ K ($150\text{ K} < T < T_{CO}$).

IV. DISCUSSION

The coexistence of ferromagnetic metallic and antiferromagnetic CO states in doped manganites is being extensively investigated within the framework of double-exchange theory, phase segregation and electronic phase separation phenomena. $Pr_{2/3}Ca_{1/3}MnO_3$ is, within this context, a paradigmatic compound representative of the intermediate-x region in samples of a moderate distortion (bandwidth placed close to the boundary that separates metallic and insulating low-temperature behavior). A feature to be emphasized in the present compound is that the two cations sharing the A site in the structure have very similar ionic sizes (1.126 Å[Pr^{3+}] and 1.12 Å[Ca^{2+}]). This represents a very important advantage or simplification because it allows disregard the strain effects and local structural modulations due to size distribution and mismatch present in most of the $(Ln,Ln')_{1-x}A_xMnO_3$ compounds with coexistence of FM and AFM ordering [(La, Y), (La, Tb), etc]. Local strain effects with origin at the size distribution of the A-site cations are thus completely minimized in the present compound. Hence, the presence of structural inhomogeneities in this case should be ascribed to an inhomogeneous ground-state at a microscopic level (charge-delocalized versus charge-localized or charge-ordered states).

The observation of the coexistence of FM and AFM in $Pr_{2/3}Ca_{1/3}MnO_3$ comes from the evolution of the integrated intensities shown in Fig. 1. The $(h/2\ k/2\ 0)$ and $(h/2\ k\ 0)$ AFM intensities continue to grow below T_C. From ND data there is no evidence for a significant coupling between the FM and AFM phases in $Pr_{2/3}Ca_{1/3}MnO_3$. In addition, the characteristic broadening of the AFM peaks $(\frac{1}{2}\ 0\ l)$ associated with the Mn^{3+} sublattice observed in $Ln_{1/2}Ca_{1/2}MnO_3$ compounds is not appreciated in $Pr_{2/3}Ca_{1/3}MnO_3$. The AFM Bragg peaks are very narrow, similar to the nuclear ones (see Fig. 6). This is not surprising if one considers that the magnetic domain boundaries breaking the magnetic coherence of the Mn^{3+} sublattice (magnetic spin flip for $x=\frac{1}{2}$) are likely associated with structural a-b twins at Mn^{4+} sites. They break the coherence of the orbital ordering but not that of the charge ordering with $x=\frac{1}{2}$. For $x=\frac{1}{3}$ a fraction of ideally Mn^{4+} sites is now occupied by the extra e_g electrons, frustrating the mechanism of twin formation. In any case, the important point is that the coherence length of the AFM domains is, from ND data, of the order of >500–1000 Å. The FM Bragg intensity at the (0 0 2) and (1 1 0) peaks have been shown in Fig. 6. From the difference pattern at both sides of T_C we estimate that the FM coher-

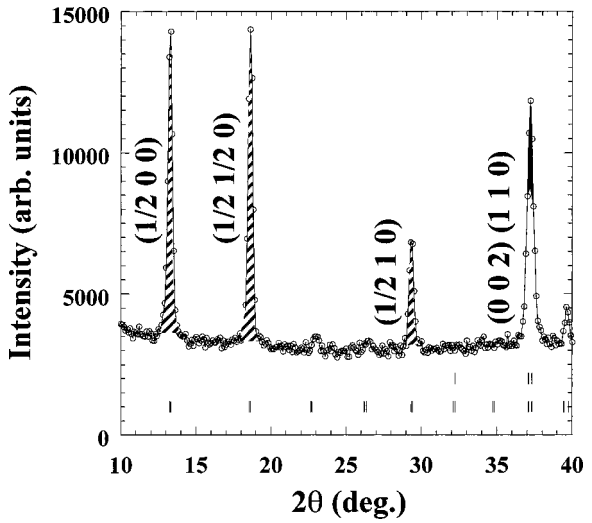

FIG. 6. Low angle detail of the ND data illustrating the width of the main magnetic peaks [AFM (stripes) and FM (black) Bragg intensities at $T=68$ K].

ence length should be at least of the order of several hundreds of angstroms. Therefore, in a first approximation the compound presents large AFM domains associated with CO regions (origin of the observed structural (2 $\frac{3}{2}$ 0) superlattice peak), which coexist with extensive regions (mesoscopic rather than nanoscopic) with a ferromagnetic ordered component. In addition to this, it is important to emphasize that the volume proportion containing magnetic disorder should be very high. Experimentally this is supported by the low values of the ordered moments at low temperature (between 1 and $1.5\mu_B$ below the saturation values). Although the regions with magnetic disorder may be ascribed to domain boundaries separating well ordered FM and AFM domains, we will demonstrate later that this picture is not supported by experimental data.

Before discussing the muon relaxation results we should recall that the dynamical relaxation rate $\lambda(T)$ in orthoferrites showed minima and peaks, uncorrelated with the proper phase transitions.[17] The reason is that the muon starts slow diffusion at about 250 K. Unlike these muon studies in orthoferrites, we found no evidence for muon diffusion in $Pr_{2/3}Ca_{1/3}MnO_3$ in the temperature range of our study (up to 350 K). We are thus led to assume that possible effects due to muon diffusion can be neglected in the present compound below the charge-ordering transition.

In the following we will focus on the important implications that the μSR results and the observed spin dynamics have with respect to the two most probable scenarios: (i) The first scenario consists of CO regions, with a long range coherence and AFM ordered, spatially separated from the FM domains or large clusters where the JT polarons have not frozen and which may have a broad size distribution. In the framework of ''phase separation'' models, the second regions may be richer in e_g electrons than the first. (ii) The second scenario is closer to a canted magnetic arrangement where AFM and FM regions have a spatial distribution strongly overlapped. Namely, the volume occupied by domain boundaries is not negligible but, on the contrary, variable size clusters of the minority phase are densely scattered within the majority phase in a large fraction of the sample.

In oxides the coupling strength between muon and electron spins (either dipolar or hyperfine) depends on the particular coupling between the electronic spins (FM or AFM). In polycrystalline charge-ordered manganites with the ideal hole concentration $Mn^{4+}/Mn^{3+}=1$ (commensurate), the exponential relaxation rate λ in the PM/CO phase is always within the interval $\lambda \sim 0.04-0.06\,\mu s^{-1}$, even very close to but above T_N.[16,18,19] We call to mind that these values are significantly smaller than the relaxation values found in the paramagnetic phase of ferromagnetic Ln-Mn-O specimens.[16,18–22] In polycrystalline metallic manganites the relaxation λ falls within the interval 0.10–0.30 μs^{-1} above T_C.[16,18–21] In addition, the second relevant feature of $\lambda(T)$ in the paramagnetic regime of $x=\frac{1}{2}$ samples is a characteristic relative maximum coinciding with the CO transition.[16,18,19] As occurs with the magnetic susceptibility, the spin-lattice relaxation $\lambda(T)$ drops below T_{CO} due to the substitution of AFM by FM interactions.

We turn to the $x=\frac{1}{3}$ sample noting that both these two main characteristic features of the muon relaxation in $x=\frac{1}{2}$ CO manganites differ from the spin dynamics observed in $Pr_{2/3}Ca_{1/3}MnO_3$. (i) It is apparent from Fig. 3 that the relaxation rate of $Pr_{2/3}Ca_{1/3}MnO_3$ does not present a clear local maximum coinciding with the real space ordering of Mn^{3+} and Mn^{4+} ions around 220 K. (ii) Furthermore, the absence of a local maximum at T_{CO} agrees with the fact that muon relaxation in $Pr_{2/3}Ca_{1/3}MnO_3$ is clearly dominated by a mechanism based on FM instead of AFM Mn-Mn correlations. This is shown in Fig. 3, where the measured relaxation rates are remarkably larger than the characteristic values found in $x=\frac{1}{2}$ compounds. Below T_{CO} the values of λ in this figure are totally comparable to the relaxation found in FM metallic Ln-Mn-O samples (for instance, $La_{2/3}Ca_{1/3}MnO_3$).[16,18–22] Consequently, the FM Mn-Mn correlations are the dominant relaxation mechanism of the muon polarization at least below T_{CO} and, therefore, clearly above the Néel temperature.

At this point it is convenient to realize that the AFM arrangement of the $x=\frac{1}{3}$ and $x=\frac{1}{2}$ CO phases is not strictly identical. In the pseudo-CE magnetic structure of the former the AFM Mn-O layers are ferromagnetically coupled along the c axis, whereas this coupling is antiferromagnetic for $x=\frac{1}{2}$ (CE magnetic structure). As mentioned in Ref. 3, this is likely the result of a sizeable number of Mn^{3+} ions at the Mn(II) site (extra e_g electrons) having the $d_{3z^2-r^2}$ orbital along the c direction instead of parallel to the a-b layer. By looking at the tiny ($\frac{1}{2}$ 0 1) and ($\frac{1}{2}$ $\frac{1}{2}$ 1) intensities in Fig. 6, there is a very small fraction of cells with a-b layers AFM coupled but that is negligible when compared with the intensity of ($\frac{1}{2}$ 0 0) and ($\frac{1}{2}$ $\frac{1}{2}$ 0) peaks. The magnetic coupling between layers has some implications because the most probable muon site, as determined on orthoferrites[17] and in pure $LaMnO_3$,[21] is in the $z=\frac{1}{4}$ mirror plane between Mn layers, 1 Å from the apical oxygen O(1) of the Mn-O(1)-Mn apical bond. Namely, the observed FM relaxation mechanism might thus be related to the FM coupling between adjacent a-b layers, present in the CO phase. It is worthwhile noticing that if this was the main source of depolarization in the CO regions an abrupt drop of the relaxation rate should occur below T_N. Interestingly, Fig. 3 confirms that such a drop does not occur, signaling the unlikely CO origin of the

FM relaxation. Furthermore, the close relationship between the FM relaxation mechanism below T_{CO} and the phase that orders below T_C, is also confirmed by the following result shown in Fig. 3: the peaked shape of $\lambda_s(T)$ is centered at T_c, not at T_N as happens in homogeneous CO samples. Consider the scenario of two magnetic subsystems (FM and AFM), spatially separated by domain walls of reduced extension (disordered and/or canted). Assuming a relative domain distribution similar to the experimental $[m_{\mathrm{AFM}}]^2/[m_{\mathrm{FM}}]^2$ ratio, or even below, an appreciable anomaly in the relaxation rate would occur at the Néel temperature. Actually, the absence of a relative maximum in $\lambda_s(T)$ at the Néel point is another key result signaling the dominance in the sample of zones with fluctuating internal fields caused by FM correlated Mn moments. Close to T_c the evolution of $\lambda_s(T)$ in Fig. 3 describes the critical slowing down in the spin dynamics as the FM freezing is approached.

In agreement with the magnetic diffraction data, some of the muon results presented above could be taken as evidence for the existence of FM domains independent or decoupled from the AFM regions. This is the case of the FM correlations observed, when cooling the sample, between T_{CO} and T_N while the system approaches the critical slowing down leading to the AFM transition. In the scenario of spatially separated FM and AFM zones and neglecting muon diffusion, the final relaxation would be the sum of the contributions from muons implanted in each zone. The depolarization of muons in FM zones is more rapid than in pure AFM zones. Thereby, the contribution to $G_z(t)$ from the first is expected to decay more rapidly than that from the AFM zones. Nevertheless, the relaxation values below T_{CO} confirm that the predominant contribution to $G_z(t)$ comes from muons seeing FM correlations. Since muons in the sample are randomly distributed, we are thus led to conclude that below T_{CO} the volume fraction occupied by cells that experience FM fluctuating fields is very large, clearly much larger than the corresponding to pure AFM correlations. The importance of the FM and AFM interpenetrated regions in this compound is thus confirmed. This fact seems to be very akin to the lack of two well defined cells in neutron and synchrotron diffraction data.[3] Instead, lattice strain is particularly apparent in the diffraction patterns below T_{CO}.

In Fig. 7(b) we show the temperature dependence of the relative fraction of muons feeling a local static field at their site. This fraction, obtained from the evolution of the initial asymmetry, is related to the relative volume fraction exhibiting some degree of magnetic order. For comparison, the dependence for $Pr_{0.5}Ca_{0.5}MnO_3$ is also shown in the figure and the temperature is referred to the Néel point. For $x=\frac{1}{3}$ static fields develop over the interval 100–180 K. The existence of frozen moments in the whole volume is only attained close to but below T_c. Moreover, it is worthwhile noticing that in contrast with the abrupt behavior at the onset of local AFM order in the manganite with $x=\frac{1}{2}$, the onset in $Pr_{2/3}Ca_{1/3}MnO_3$ is very rounded. A significant change of slope seems to occur close to T_c. In fact a very small fraction of this sample exhibits local order below ~180 K [above the emergence of magnetic Bragg peaks; inset of Fig. 7(b)]. From the evolution of the entropy change $\Delta s(T)$ shown in Fig. 4(b) this is the temperature at which the CO transition has come to completion. This represents an additional confirmation of intrinsic structural and magnetic inhomogeneities in the sample. The round transition in Fig. 7(b) may be ascribed to a distribution of Néel temperatures with origin at the lattice strain and/or possibly driven by local fluctuations of the density of e_g electrons. On another hand, a very low density of tiny (nanometric) clusters with trapped electrons and blocked moments that may have nucleated through the inhomogeneous CO transition could be the origin of the small ordered fraction detected below 180 K.

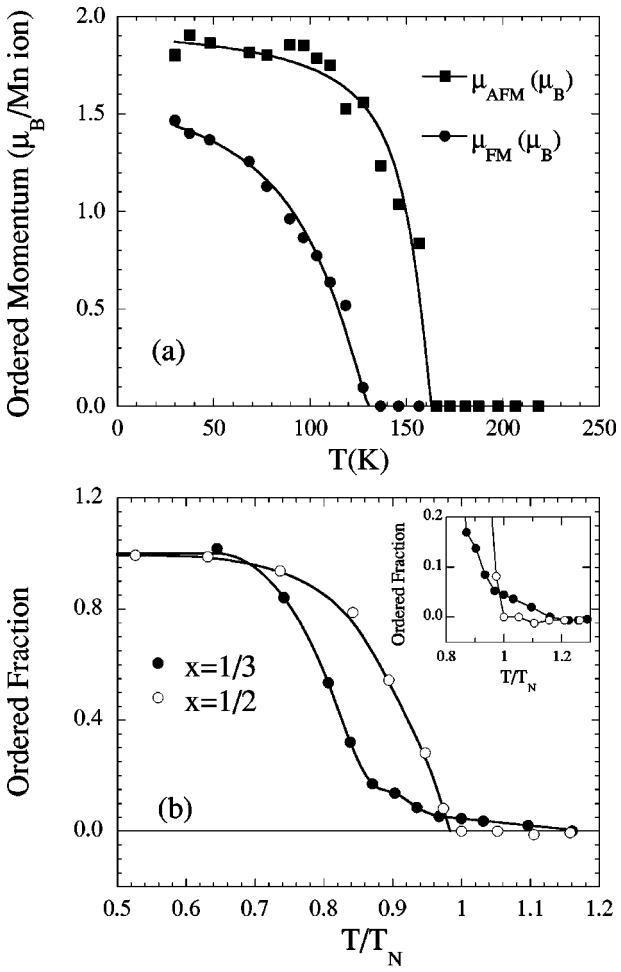

FIG. 7. (a) Thermal dependence of the ordered FM and pseudo-CE AFM magnetic moments for $Pr_{2/3}Ca_{1/3}MnO_3$ (from ND data). (b) Thermal dependence of the fraction of muons sensing a static magnetic field in incommensurate $Pr_{2/3}Ca_{1/3}MnO_3$ (temperature refers to the Néel transition point: $T_N=155$ K). For comparison the same dependence is shown for the commensurate $Pr_{1/2}Ca_{1/2}MnO_3$ case ($T_N=190$ K). Temperature markers correspond to $x=\frac{1}{3}$. Inset: different evolution around T_N of the $x=\frac{1}{3}$ and $x=\frac{1}{2}$ compounds.

Finally, although the results suggest that the spatial distribution of AFM and FM regions strongly overlaps, the ground state is clearly far from a quasihomogeneous canted magnetic arrangement. Additional information that suggests significant local fluctuations of the density of carriers as a source of disorder comes from the DSC measurements [see Fig. 4(b)]. The entropy change through T_{CO} ($\Delta s \approx 0.06R$) is considerably smaller than the expected change associated to the ordering of the e_g electrons in this system: $\Delta s_{\mathrm{theor}} \approx 0.32R$. Namely, $\Delta s < 1/5 \Delta s_{\mathrm{theor}}$. The theoretical estima-

tion comes from the assumption that above T_{CO} the e_g electrons are freely placed among the Mn positions, while below T_{CO} all the Mn(II) positions are occupied by e_g electrons and the Mn(I) sites are randomly occupied by the remaining electrons. This assumption is very crude but such a huge difference between these two values cannot be easily justified without significant local inhomogeneties in the electronic distribution and disorder. To illustrate this it is worth mentioning that numerical integration of the specific heat of $La_{0.35}Ca_{0.65}MnO_3$ reported in Ref. 23 reveals an entropy change through the CO transition clearly closer to its theoretical value $\Delta s \sim 1/2\Delta s_{theor}$ [here Δs_{theor} has been calculated taking as low-temperature phase the CO proposed for $La_{1/3}Ca_{2/3}MnO_3$ (Ref. 24).

V. SUMMARY

The unusual properties and mixed nature of $Pr_{2/3}Ca_{1/3}MnO_3$ have been investigated combining neutron diffraction, muon spin relaxation, magnetic, and calorimetric techniques. Analysis of the calorimetric data evidences a high degree of disorder below the CO transition. *A priori*, one should expect less disorder in compounds with charge-orbital ordered state of very high symmetry, such as $Pr_{2/3}Ca_{1/3}MnO_3$, than in systems that order with lower symmetry, such as $Ln_{1/3}Ca_{2/3}MnO_3$. Conversely, the disorder kept in the system below T_{CO} is much more pronounced in $Pr_{2/3}Ca_{1/3}MnO_3$ than in $Ln_{1/3}Ca_{2/3}MnO_3$. This disorder is not related to chemical disorder or physical defects, but it is of electronic origin, probably due to the fact that FM metallic and AFM CO states are, in this case, quasidegenerate in energy.[3] There is no doubt that a thermally driven spin reorientation must be ruled out in favor of two coexisting phases of similar energy.

The μSR technique has been used to get information on the real spatial distribution of the FM and AFM regions. The microscopic development of static FM moments agrees within the error with the appearance of FM Bragg intensity in the ND data. Muon relaxation in $Pr_{2/3}Ca_{1/3}MnO_3$ does not exhibit the thermal dependence characteristic of commensurate charge-order $Ln_{1/2}Ca_{1/2}MnO_3$ compounds. The spin-lattice relaxation $\lambda(T)$ does not drop below T_{CO}. Below T_{CO} the dominant relaxation mechanism of the muon polarization is based on FM Mn-Mn correlations and the relaxation rate is peaked at T_C instead of T_N. Persistent FM correlations are clearly visible between T_N and T_{CO} while the system approaches the AFM freezing. Instead of confined mesoscopic FM clusters and in consistency with noticeable lattice strain below T_{CO}, these results suggest a model where FM and AFM regions have a spatial distribution strongly interpenetrated. In agreement with the results of Ref. 6, the large coherent CO regions seems to contain structural and magnetic defects densely scattered. The nucleation of structural disorder and magnetic frustration is favored by the quasidegeneracy of the ground state, the particular orbital occupancy of the extra e_g electrons, and likely local fluctuations in their spatial distribution.

We would finally like to mention that the picture considered above is an static approximation. From a dynamic point of view, the possibility of local slow fluctuations between the CO and the FM states associated with the jumps from site to site of the excess e_g electrons (local AFM-FM transitions entropically activated) requires further experimental efforts.

ACKNOWLEDGMENTS

The authors acknowledge financial support by the CICyT (MAT97-0699), MEC (PB97-1175), Generalitat de Catalunya (GRQ95-8029) and the EC through the ''Oxide Spin Electronics (OXSEN)'' network (TMR). The ISIS, ILL, and LLB laboratories are acknowledged for making available the beam time. The EC HCM program for Large Scale Facilities supported μSR measurements at ISIS.

*Author to whom correspondence should be addressed. Electronic address: garcia.munoz@icmab.es

[1] H. Yoshizawa, H. Kawano, Y. Tomioka, and Y. Tokura, Phys. Rev. B **52**, R13 145 (1995).
[2] V. Kiryukhin, D. Casa, J. P. Hill, B. Keimer, A. Vigilante, Y. Tomioka, and Y. Tokura, Nature (London) **386**, 813 (1997).
[3] D. E. Cox, P. G. Radaelli, M. Marezio, and S.-W. Cheong, Phys. Rev. B **57**, 3305 (1998).
[4] D. Casa, V. Kiryukhin, O. A. Saleh, B. Keimer, J. P. Hill, Y. Tomioka, and Y. Tokura, connd-mat/9809242 (unpublished).
[5] Y. Tomioka, A. Asamitsu, H. Kuwahara, Y. Moritomo, and Y. Tokura, Phys. Rev. B **53**, R1689 (1996); Y. Tomioka, A. Asamitsu, Y. Moritomo, and Y. Tokura, J. Phys. Soc. Jpn. **64**, 3626 (1995).
[6] A. Anane, J.-P. Renard, L. Reversat, C. Dupas, P. Veillet, M. Viret, L. Pinsard, and A. Revkolevski, Phys. Rev. B **59**, 77 (1999).
[7] A. Asamitsu, Y. Tomioka, H. Kuwahara, and Y. Tokura, Nature (London) **388**, 50 (1997).
[8] Y. Morimoto, H. Kuwahara, Y. Tomioka, and Y. Tokura, Phys. Rev. B **55**, 7549 (1997).
[9] M. Fiebig, K. Miyano, Y. Tomioka, and Y. Tokura, Science **280**, 1925 (1998).
[10] K. Miyano, T. Tanaka, Y. Tomioka, and Y. Tokura, Phys. Rev. Lett. **78**, 4257 (1997).
[11] M. Hervieu, A. Barnabé, C. Martin, A. Maignan, and B. Raveau, Phys. Rev. B **60**, R726 (1999).
[12] A. Anane, B. Raquet, S. von Molnár, L. Pinsard-Godart, and A. Revkolevski, cond-mat/9910204 (unpublished).
[13] J. Rodríguez-Carvajal, Physica B **192**, 55 (1993).
[14] A simplified version of the calorimeter is described in L. Mañosa, M. Bou, C. Calles, and A. Cirera, Am. J. Phys. **64**, 283 (1996).
[15] Z. Jirák, S. Krupicka, Z. Simsa, M. Dlouha, and S. Vratislav, J. Magn. Magn. Mater. **53**, 153 (1985).
[16] A. LLobet, J. L. García-Muñoz, C. Frontera, M. Respaud, H. Rakoto, and J. S. Lord, Physica B (to be published).
[17] E. Holzschuh, A. B. Denison, W. Kundig, P. F. Meier, and B. D. Patterson, Phys. Rev. B **27**, 5294 (1983).
[18] J. L. García-Muñoz, A. Llobet, C. Frontera, J. Fontcuberta, X. Obradors, and C. Ritter, J. Magn. Magn. Mater. **196–197**, 477 (1999).
[19] J. L. García-Muñoz, A. Llobet, C. Frontera, and C. Ritter, J. Appl. Phys. **85**, 5639 (1999).

[20] R. H. Heffner, L. P. Le, M. F. Hundley, J. J. Neumeier, G. M. Luke, K. Kojima, B. Nachumi, Y. J. Uemura, D. E. MacLaughlin, and S.-W. Cheong, Phys. Rev. Lett. **77**, 1869 (1996).

[21] R. de Renzi, G. Allodi, M. Cestelli Guidi, G. Guidi, M. Hennion, L. Pinsard, and A. Amato (unpublished).

[22] R.H. Heffner, D. E. MacLaughlin, G. J. Nieuwenhuys, T. Kimura, G. M. Luke, Y. Tokura, and Y. J. Uemura, Phys. Rev. Lett. **81**, 1706 (1998).

[23] A. P. Ramírez, P. Schiffer, S.-W. Cheong, C. H. Chen, W. Bao, T. T. M. Palstra, P. L. Gammel, D. J. Bishop, and B. Zegarski, Phys. Rev. Lett. **76**, 3188 (1996).

[24] M. T. Fernández-Díaz, J. L. Martínez, J. M. Alonso, and E. Herrero, Phys. Rev. B **59**, 1277 (1999); P. G. Radaelli, D. E. Cox, L. Capogna, S.-W. Cheong, and M. Marezio, *ibid.* **59**, 14 440 (1999).